FULL CHARACTERIZATION OF NEAR-SURFACE FLAWS WITH MULTIMODE STRAIGHT-BEAM TRANSDUCERS

G. J. Gruber
Southwest Research Institute
P.O. Drawer 28510
San Antonio, Texas 78228-0510

S. R. Burger
General Electric Company
P.O. Box 1072
Schenectady, New York 12301

INTRODUCTION

Reliable and accurate characterization as to type (cracks vs. others), location (highly stressed zone or not), and size of potential flaws in cladded pressure vessels by ultrasonic methods ensures the integrity of these structures. Vessel integrity is primarily affected by the presence of fatigue cracks in the highly stressed near-surface regions (Zones 1 and 2). While there have been some new high- and low-beam multimode transducer developments for characterizing Zone 2 (underclad) and Zone 3 (deeply buried) flaws, respectively [1,2], emphasis has recently been placed upon fully characterizing manufacturing flaws in the cladding (Zone 1) because they can initiate fatigue cracks.

Conventional single- or dual-element straight-beam ultrasonic transducers have difficulties in seeing just below the surface for detection and producing, for sizing, resolvable and asynchronous (separately peaking) main and satellite pulses from the top and bottom of a small (less than 2 mm deep) inclad flaw. These limitations of existing technology motivated Southwest Research Institute to develop the hybrid (high/low-beam) SLIC-30 and SLIC-45 multimode transducers discussed in this paper.* As demonstrated, these practically straight-beam transducer designs permit the full characterization of manufacturing as well as service-induced inclad flaws. The remote ultrasonic inspection system which incorporates

*The patented SLIC transducers use shear and longitudinal ultrasonic waves simultaneously for material inspection and flaw characterization.

Review of Progress in Quantitative Nondestructive Evaluation, Vol. 12
Edited by D.O. Thompson and D.E. Chimenti, Plenum Press, New York, 1993

the qualified SLIC-30/45 procedures is able to reliably detect and identify as well as accurately locate and size inclad flaws with only two transducer modules.

PRINCIPLES OF SLIC-30 OPERATION

The inclad flaw of interest is a fatigue crack contained in the YZ (X=0) plane of Fig. 1(a) which is perpendicular to the inspection surface (Z=0). The vertical distances to the flaw top and bottom are denoted by Z_1 and Z_2, respectively, giving flaw depth d as Z_2-Z_1. In contrast to the SLIC-40 detection module [2], the SLIC-30 was especially designed to enhance the inspection system's detection, identification, and Z_1/d estimation capabilities for small inclad flaws. The piezoelectric crystals A and B, one mounted behind the other in a common housing, are connected to an ultrasonic instrument operated in the transmit-receive mode. Probe B transmits a high-angle longitudinal wave (high beam L_b) and an ineffective low-angle shear wave (low beam S_b). For all practical purposes, probe A is a straight-beam transducer, since it is "tuned" to receive 10-degree L waves (L_a channel) and 5-degree S waves (S_a channel). The interaction of the transmitted high beam with the inclad crack results in two L-channel signals [pulses 1 and 2 in Fig. 1(b)] and two S-channel signals (pulses 1S and 2S, not shown).

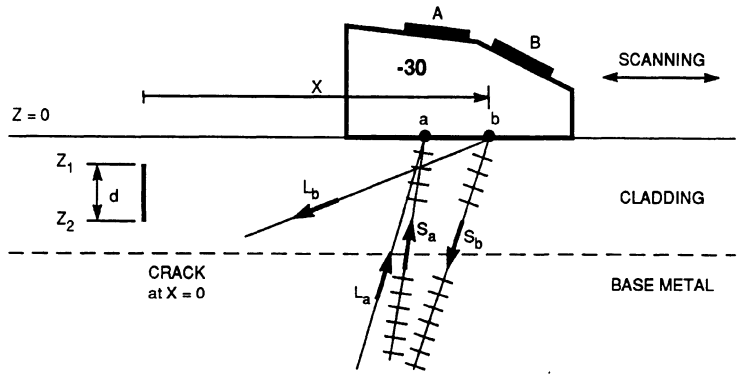

(a) Transmitted (L_b, S_b) and received (L_a, S_a) beams

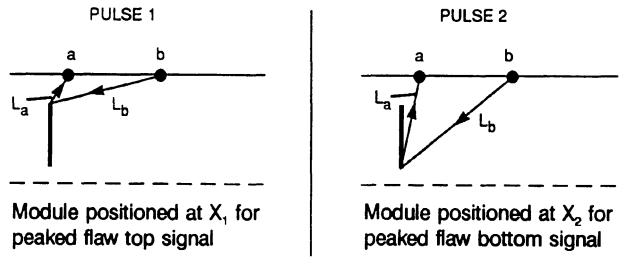

(b) Ray paths for the L-wave pulses

Fig. 1. Interaction of the transmitted longitudinal high beam (L_b) of the SLIC-30 with an inclad crack resulting in up to four low-beam pulses (one L wave and one S wave from each crack extremity). These pulses are labeled 1 (shown), 1S, 2 (shown), and 2S. The last pulse is generally not observed.

In case of a crack or lack-of-fusion flaw, both pulses 1S and 2S are generally absent from the received pulsetrain. In contrast, a strong pulse 1S may be observed in addition to pulse 1 from the top of a slag, porosity, or lack-of-bond (clad unbond) flaw.

Flaw sizing in the throughwall direction is the primary function of the SLIC-30. At the X_1 module position shown on the left in Fig. 1(b), the center of the L_a beam is aimed at the flaw top by peaking pulse 1. This is the essence of the Peak Echo Technique (PET). The PET estimate for flaw ligament Z_1 is obtained simply by reading the position of the peaked pulse 1 on the instrument screen calibrated directly in millimeters of throughwall distance. Similarly, the PET estimate for Z_2 is obtained by aiming the L_a beam at the flaw bottom as shown on the right of Fig. 1(b) and reading the screen distance under the peaked pulse 2. The PET estimate for the flaw depth is obtained simply by subtracting the Z_1 estimate from the Z_2 estimate.

The Satellite-Pulse Observation Technique (SPOT) provides a more accurate flaw depth estimate because it is based solely on predictable relative time-of-flight (doublet separation) measurements between the main pulse (flaw top signal) and the satellite pulse (flaw bottom signal). As shown in Fig. 2 for a set of notches located 8 mm below the surface, the measured doublet separation is a linear correlate of flaw depth. Unlike the PET depth estimates, the SPOT estimates are independent of the unpredictable pulse amplitudes. The unknown dependence of doublet separation τ on module position X and flaw ligament Z_1, in addition to its desired linear (Fig. 2) dependence on flaw depth d, has necessitated in the past the fabrication of calibration blocks containing side-milled notches of varying Z_1 and d

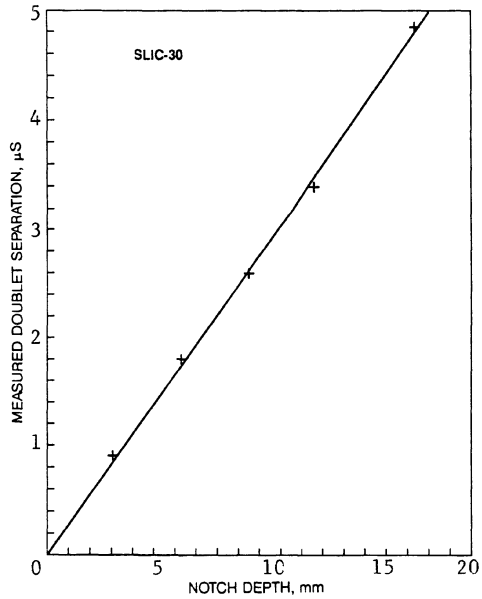

Fig. 2. Plot illustrating the linear relationship between the measured SLIC-30 doublet (pulses 1 and 2) separation and the depth of a set of underclad notches located 8 mm below the surface.

to aid in the flaw-sizing process. The equations derived below, which predict the variation of pulse position P_0 with module position X for a family of point sources located a distance Z_0 below the surface, not only result in significant block fabrication cost savings but also permit partial automation of the flaw-depth estimation process.

The three sound paths (rays ba, bf, and fa) needed for modeling the L-to-L wave interaction of the SLIC-30 with a small side-drilled hole (point source) are shown on the left of Fig. 3. Note that the pulse returning from the top of a surface-connected notch along reference ray R marks the Z=0 origin of the instrument screen's time base calibrated in mm for direct PET Z_1 and Z_2 readings. Relative to this reference pulse, the time of flight for the pulse reflected by the hole is given by

$$T_o(X;Z_o) = (U+V-R)/c \tag{1}$$

where

$$U = (Z_o^2 + X^2)^{1/2} \tag{1a}$$

and

$$V = [Z_o^2 + (X-R)^2]^{1/2}. \tag{1b}$$

Here, c is the L-wave velocity (=5.9 mm/μsec for steel pressure vessels). For the SLIC-30 used in the model-development experiments, the best linear fit between predicted and measured doublet separations was obtained by choosing 10 mm for R (a realistic value).

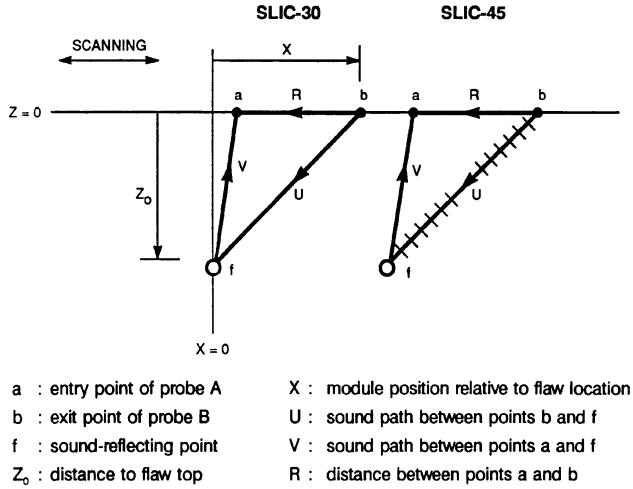

Fig. 3. The three rays (R, U, and V) involved in the production of the flaw top signal as a result of scanning the SLIC-30/45 over a side-drilled hole parallel to the Y axis.

PRINCIPLES OF SLIC-45 OPERATION

A schematic drawing of the second straight-beam multimode transducer module is shown in Fig. 4(a). In this case, a transmitted high-angle shear wave (high-beam S_b) causes the crack to launch almost straight (vertical) diffracted L and S beams from both crack top and bottom in the direction of Probe A which is, again, most sensitive to 10-degree L waves and 5-degree S waves. The ray paths involved in the production of the mode-converted L-channel waves (pulses 1 and 2) are shown in Fig. 4(b) (see also the right side of Fig. 3). Experience to date with the SLIC-45 indicates that the S-to-L wave interaction with the flaw bottom produced reliable pulse 2 satellites only for about half of the test flaws (see column 6 in Table 1). The S-to-S wave interaction with the flaw bottom is apparently too weak to produce readily observable satellite pulses. Hence, flaw ligament estimation by PET is the primary function of the SLIC-45.

The three rays needed for modeling the S-to-L wave interaction of the SLIC-45 with a point reflector are shown on the right of Fig. 3. The variation of pulse position with module position for a given reflector location is predicted by

$$P_o(X;Z_o) = (V-R)/c + U/v \qquad (2)$$

where v is the S-wave velocity (= 3.2 mm/μsec for steel vessels). The value of R, which gives the best agreement between the measured and calculated [Eq. (2)] pulse trajectories for a wide Z_0 range, is yet to be determined.

Table 1. Comparison of SLIC-30/45 flaw ligament and depth estimates with the results of metallographic sectioning.

Flaw Type[1]	Flaw Ligament, mm			Flaw Depth, mm		
	SLIC-30	SLIC-45	Actual	SLIC-30	SLIC-45	Actual
LF	6.9	6.9	7.4	2.5	2.6	2.4
LF	2.5	1.3	0.4	2.3	2.5	2.5
SL	8.0	8.5	9.3	1.6	1.5	0.4
LB	7.8	7.6	8.2	1.5	1.7	1.7
LF	8.4	8.1	9.2	1.4	1.5	0.5
LB	8.0	8.0	6.8	---	1.3	2.4
SL	6.4	6.3	6.7	3.0	2.0	1.5
VF	3.3	3.0	3.3	2.3	---	2.8
VF	3.3	3.4	2.9	1.1	---	1.3
VF	6.4	6.4	5.6	1.0	---	1.7
CR	1.0	0	1.1	9.7	---	11.2
LF	9.0	---	8.7	14.5	---	13.5
SL	14.0	13.5	13.1	2.0	2.8	4.8
SL	11.3	12.0	10.8	11.5	---	14.1
CR	31.0	30.0	29.5	7.0	7.0	6.0

[1]CR = crack, LB = lack of bond, LF = lack of fusion, SL = slag, VF = volumetric flaw

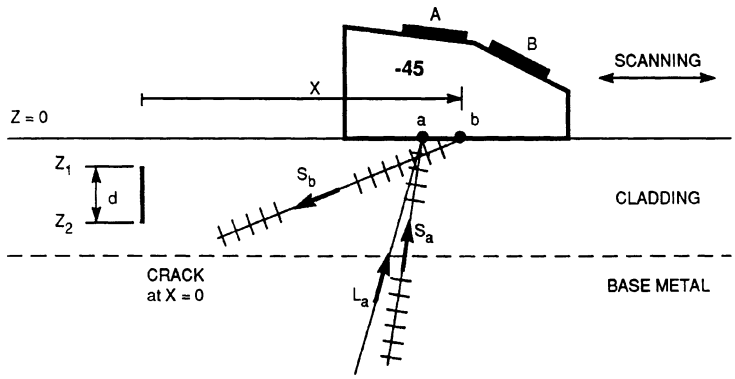

(a) Transmitted (S_b) and received (L_a, S_a) beams

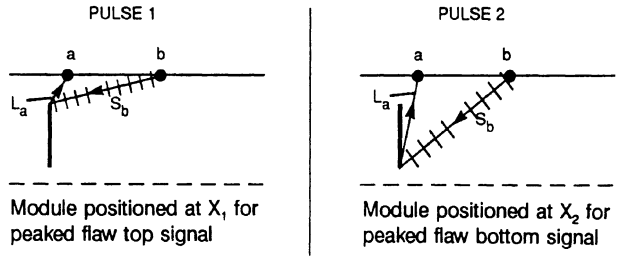

(b) Ray paths for the L-wave pulses

Fig. 4. Interaction of the transmitted shear high beam (S_b) of the SLIC-45 with an inclad crack resulting in up to four low-beam pulses (one L wave and one S wave from each crack extremity). These pulses are labeled 1 (shown), 1S, 2 (shown), and 2S. The flaw bottom signals are generally not observed.

RESULTS

Four intentionally flawed specimens containing a total of fifteen near-surface flaws (eleven inclad and four base-metal flaws, Table 1) were available to qualify the SLIC-30/45 flaw characterization procedures. It was established that data from one module must be confirmed by data from the other module (if possible) before data analysis. Amplitude, time of flight (screen position), and phase were the recorded signal parameters for each identified pulse. Module positions X_1 and X_2 corresponding to the Z_1 and Z_2 readings were also recorded. At the conclusion of the ultrasonic measurements, the flaws were verified for flaw type, ligament, and depth by metallographic sectioning.

The flaw type was determined on the basis of the results of phase comparison and echo strength/structure/persistence/dynamics tests. Since a lack of bond/fusion (LB/LF) and a slag inclusion are often the same welding flaw, it is perhaps not surprising that three of the LB/LF inclad flaws were classified slag inclusions. The other twelve flaws were classified correctly.

As shown in Table 1 and Figs. 5 and 6, the ultrasonic task to obtain a consistent (repeatable) set of PET Z_1 and Z_2 and SPOT d measurements was successfully

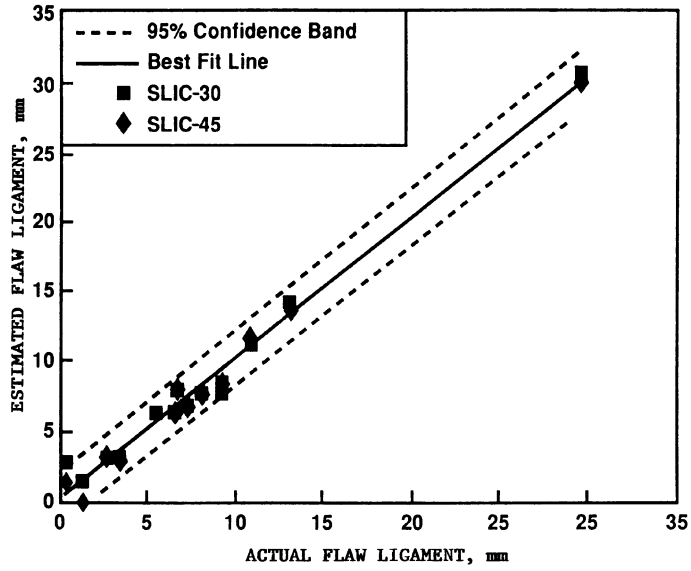

Fig. 5. Correlation of the SLIC-30/45 ligament (Z_1) estimates for the Table 1 near-surface flaws with actual flaw ligaments.

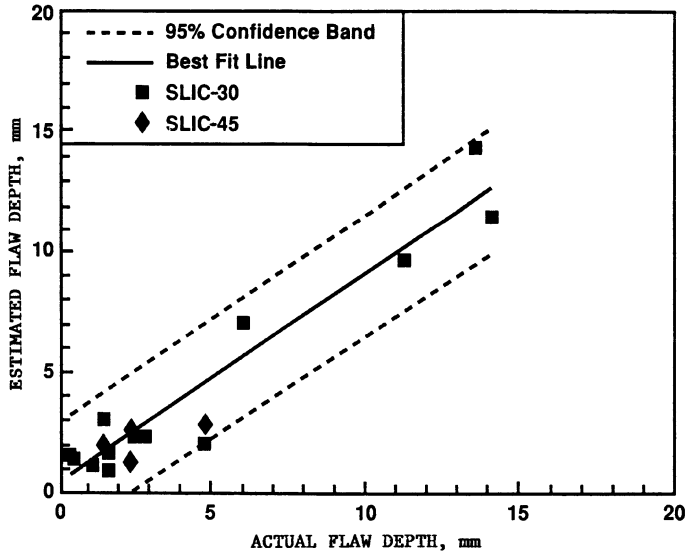

Fig. 6. Correlation of the SLIC-30/45 depth (d) estimates for the Table 1 near-surface flaws with actual flaw depths.

accomplished. To obtain a conservative estimate for the upper Z location coordinate (ligament) of a detected flaw, one must subtract 1.5 mm from the ultrasonic estimate. The conservative flaw depth estimate is, on the other hand, obtained by adding 2 mm to its ultrasonic estimate. Inaccuracies of this magnitude are quite acceptable in fracture-mechanics predictions of the remaining lifetime of a flawed pressure vessel.

CONCLUSIONS

The objective of the reported work was to replace the conventional straight-beam ultrasonic transducers (i.e., the pulse-echo probe with a "dead zone" and the dual probe without any echo-dynamics/modeling features) with a small set of transducers capable of fully characterizing the flaws potentially present in the cladding of operating pressure vessels. We have demonstrated that only two SLIC modules are needed to reliably detect and identify fatigue cracks, slag inclusions, and lack of bond/fusion flaws and estimate their ligaments and depths with acceptable inaccuracies. The SLIC-30/45 modules yield high signal-to-noise ratios and near maximum achievable doublet separations for detecting and sizing, respectively, small flaws with ligaments ranging from about 30 mm all the way to the surface ($Z_1 = 0$). One opportunity has already occurred for implementing the automated SLIC-30 procedures in the field [3].

REFERENCES

1. G. J. Gruber, D. R. Hamlin, H. L. Grothues, and J. L. Jackson, NDT International 19, 155 (1986).

2. G. Gruber and T. Mueller, *Review of Progress in Quantitative NDE*, Vol. 8A, edited by D. O. Thompson and D. E. Chimenti (Plenum Press, New York, 1989), p. 1075.

3. Automated Nondestructive Examination of the Loviisa (Finland) Nuclear Power Plant Unit 1 Reactor Pressure Vessel, Southwest Research Institute Final Report 17-4877, San Antonio, Texas, November 1992.